Building Simulation 2005

Ninth International IBPSA Conference
Montréal, Canada
August 15-18, 2005

VALIDITY OF QUASI-STEADY CONVECTION FOR SIMULATION OF VOC SOURCE AND SINK BEHAVIOR OF POROUS BUILDING MATERIALS

Chang-Seo Lee[1], Fariborz Haghighat[1], and Wahid Ghaly[2]
[1] Department of Building, Civil, and Environmental Engineering
[2] Department of Mechanical and Industrial Engineering
Concordia University, Montreal, Canada

ABSTRACT

Volatile organic compounds (VOC) are major indoor air pollutants. Physical models that have been developed to predict VOC source (emission) and sink behavior (sorption) of building materials, commonly adopt the conventional convection approach using third-kind boundary condition assuming quasi-steady convective mass transfer in fluid (air). In this study, conjugate mass transfer models were developed to investigate the validity and application limit of the assumption. The conjugate mass transfer models consider either quasi-steady or unsteady two-dimensional laminar forced convection over a flat plate coupled with unsteady one-dimensional diffusion and sorption within the porous solid through the concentration and the flux continuities at the solid-air interface. The simulation results indicated that the quasi-steady assumption in convection mass transfer may result in significant overestimation of wall concentration or underestimation of Sherwood number in the early transfer phase; however, the errors caused by the quasi-steady assumption become less than 5 % after about 2.5 times of convection characteristic time, i.e., the time taken by a particle moving with a constant velocity to travel along the plate.

INTRODUCTION

Volatile organic compounds (VOC) emitted from various building materials and furnishings have become a growing concern due to their adverse impacts on human comfort and health. Presence of porous building materials can affects the dynamic behavior of indoor air pollutants, since they act not only as pollutant sources but also as sinks.

Several physical models have been developed to predict the VOC source and sink behavior of solid (dry) building materials. Simplified numerical simulations [Huang and Haghighat, 2002] and analytical models [Lee et al., 2003a, Huang and Haghighat et al., 2002] use conventional convection approach using third-kind boundary condition as follows,

$$-D_s \left.\frac{\partial C}{\partial y}\right|_{y=0-} = h_D \cdot (C_w - C_\infty) \qquad (1)$$

where, D_s is the effective diffusion coefficient of the material [m^2/s], C is the VOC concentration [mg/m^3], y is the space coordinate [m], h_D is the convection mass transfer coefficient [m/s], C_w is the VOC concentration at the air-solid interface [mg/m^3], C_∞ is the VOC concentration in the bulk fluid outside the convection boundary layer [mg/m^3]. This approach is much simpler than the conjugate mass transfer approach but the key issue is how to obtain accurate convective mass transfer coefficient, h_D. h_D is generally calculated from the heat-mass transfer analogy and commonly applied Sherwood number correlations for VOC source and sink behavior are those for forced convection over a flat plate as follows,

- Laminar ($Re_L < 5\times10^5$)

$$Sh_L = 0.664 \cdot Re_L^{0.5} \cdot Sc^{\frac{1}{3}} \qquad (2)$$

- Turbulent ($Re_L > 5\times10^5$)

$$Sh_L = 0.036 \cdot Re_L^{0.8} \cdot Sc^{\frac{1}{3}} \qquad (3)$$

where, Sh_L is the averaged Sherwood number ($Sh_L=h_D \cdot L/D_a$); Re_L is the Reynolds number based on the plate length ($Re_L=u_\infty \cdot L/\nu$); Sc is the Schmidt number ($Sc=\nu/D_a$); D_a is the binary molecular diffusion coefficient of air and VOC [m^2/s]; L is the length of the solid [m]; u_∞ is the air velocity outside the boundary layer [m/s]; and ν is the kinematic viscosity [m^2/s].

Applying the conventional convection approach using the commonly adopted Sherwood number correlations, contains the assumption of quasi-steady convective mass transfer. This assumption is based on that the convection characteristic time is generally much shorter than the diffusion characteristic time for VOC source/sink behavior of solid building materials. The validity of this assumption, however, has never been studied.

This study investigated the validity and the application limits of the quasi-steady convection

assumption for VOC source and sink behavior of porous building materials using two conjugate mass transfer models: unsteady one-dimensional diffusion and adsorption/desorption within a porous material coupled with 1) quasi-steady; or 2) unsteady laminar two-dimensional forced convection over a flat plate. For a comprehensive investigation, the simulations were carried out for inclusive ranges of independent parameters taken from experimental data [Haghighat et al., 2002, Meininghaus et al., 2000].

MODEL DEVELOPMENT

Governing equations

Since the mass fraction of VOCs in air is very small and the mass transfer at the fluid-solid is low, the governing equations for fluid flow can be written ignoring the presence of VOCs. For steady two dimensional flow of a constant-property Newtonian fluid, the continuity and the momentum equations, assuming a boundary layer developing in the *x*-direction, are written as follows:

Continuity equation

$$\frac{\partial u}{\partial x}+\frac{\partial v}{\partial y}=0 \qquad (4)$$

x-momentum boundary layer equation

$$u\frac{\partial u}{\partial x}+v\frac{\partial u}{\partial y}=\nu\frac{\partial^2 u}{\partial y^2} \qquad (5)$$

where, u and v are velocity components in x-direction and y-direction, respectively [m/s].

VOC convection in the fluid region is expressed in terms of the concentration boundary layer equation and is written in both quasi-steady and unsteady convection as follows.

$$\left(\frac{\partial C}{\partial t}\right)+u\frac{\partial C}{\partial x}+v\frac{\partial C}{\partial y}=D_a\frac{\partial^2 C}{\partial y^2} \qquad (6)$$

The governing equation of unsteady one-dimensional diffusion in the solid material of constant effective diffusivity including physical adsorption/desorption is

$$\varepsilon\frac{\partial C}{\partial t}+\frac{\partial C_{ad}}{\partial t}=D_s\frac{\partial^2 C}{\partial y^2} \qquad (7)$$

The sorption isotherm relates C_{ad} in terms of C, and Henry isotherm is commonly used since dry building materials are generally subjected to low VOC concentration levels,

$$C_{ad}=K\cdot C \qquad (8)$$

where, K is the Henry constant [dimensionless]. Substituting Eq. (8) into Eq. (7) gives

$$(\varepsilon+K)\frac{\partial C}{\partial t}=D_s\frac{\partial^2 C}{\partial y^2} \qquad (9)$$

The boundary conditions for momentum transfer are as follows,

at y = 0, $u = v = 0$ (10)

as $y\to\infty$, $u\to u_\infty$ (11)

The initial conditions for mass transfer are as follows,

t = 0 and y > 0, $C = C_\infty$ (12)

t = 0 and –b < y < 0, $C = C_o$ (13)

The boundary conditions for mass transfer at the fluid-solid interface follow from the fact that both mass concentration and mass flux have to be continuous,

t > 0 and y = 0, $C_{y=0^-} = C_{y=0^+}$ (14)

$$D_s\frac{\partial C}{\partial y}\bigg)_{y=0^-}=D_a\frac{\partial C}{\partial y}\bigg)_{y=0^+} \qquad (15)$$

Outside the concentration boundary layer, the concentration reaches the ambient concentration (C_∞).

t > 0 and $y\to\infty$, $C\to C_\infty$ (16)

At the bottom of the solid and at the edges, there is no mass transfer

t > 0 and y = -b $\frac{\partial C}{\partial y}=0$ (17)

Figure 1 presents the schematics of the developed conjugate mass transfer models.

Nondimensional governing equations

The governing equations, and initial and boundary conditions for mass transfer, are non-dimensionalized using the following nondimensional variables.

$$\theta=\frac{C-C_\infty}{C_o-C_\infty} \qquad t_c^{+}=\frac{t}{t_c}=\frac{t}{L/u_\infty}$$

$$x^{+}=\frac{x}{L}\quad y^{+}=\frac{y}{b} \qquad (18)$$

$$u^{+}=\frac{u}{u_\infty} \qquad v^{+}=\frac{v}{u_\infty}$$

where t_c is the convection characteristic time [s], which physically corresponds to the time taken by a particle moving with a velocity of u_∞ to travel along the plate from $x = 0$ to $x = L$.

The nondimensional system of governing equations, and initial and boundary conditions for mass transfer can be expressed as follows:

Nondimensional convection mass transfer (fluid)

$$\left(\frac{\partial\theta}{\partial t_c^{+}}\right)+u^{+}\frac{\partial\theta}{\partial x^{+}}+\frac{v^{+}}{\phi}\frac{\partial\theta}{\partial y^{+}}=\frac{1}{\phi^2\,\mathrm{Re}_L\,Sc}\frac{\partial^2\theta}{\partial y^{+2}} \qquad (19)$$

Nondimensional diffusion mass transfer (solid)

$$\left(\varepsilon+\frac{1}{(C_o-C_\infty)}\cdot\frac{\partial f}{\partial\theta}\right)\frac{\partial\theta}{\partial t_c^+}=\frac{1}{\phi^2\,\mathrm{Re}_L\,Sc\cdot\left(\frac{D_a}{D_s}\right)}\frac{\partial^2\theta}{\partial y^{+2}} \quad (20)$$

Nondimensional initial and boundary conditions for mass transfer

$t_c^+ = 0$ *and* $y^+ > 0$, $\theta = 0$ (21)

$t_c^+ = 0$ *and* $-1 < y^+ < 0$, $\theta = 1$ (22)

$t_c^+ > 0$ and $y^+ = 0$, $\theta_{y^+=0^-} = \theta_{y^+=0^+}$ (23)

$$\left.\frac{D_s}{D_a}\frac{\partial\theta}{\partial y^+}\right)_{y^+=0^-} = \left.\frac{\partial\theta}{\partial y^+}\right)_{y^+=0^+} \quad (24)$$

$t_c^+ > 0$ *and* $y^+ \to \infty$, $\theta \to 0$ (25)

$t_c^+ > 0$ *and* $y^+ = -1$ $\dfrac{\partial\theta}{\partial y^+} = 0$ (26)

$t_c^+ > 0$ *and* $x^+ = 0$ *or* $x^+ = 1$, $\dfrac{\partial\theta}{\partial x^+} = 0$ (27)

where, ϕ is thickness (b) to length (L) ratio.

The relation between t_c^+ and the Fourier number is

$$t_c^+ = Fo\cdot\frac{b^2}{D_s}\frac{u_\infty}{L} = Fo\cdot\mathrm{Re}_L\cdot Sc\cdot\frac{D_a}{D_s}\cdot\phi^2 \quad (28)$$

Numerical methods and procedures

Since the fluid flow equations are decoupled from the mass transfer equation in the proposed numerical model, the continuity and momentum boundary layer equations can be solved first. Then, the resulting flow field information can be used as input in solving the convection mass transfer equation. In this study, the velocity field is calculated from the Blasius similarity solution [White, 1991].

Once the flow field is obtained, it is introduced into the mass transfer equations, e.g. Eqs. (19) and (20), which were solved for the concentration using the control volume based finite difference method. In this study, nodes are at cell-vertices for piecewise linear interpolation structure, and the control volume faces are located midway between the nodes as shown in Fig. 2. The nodes are denoted by the upper case letters *P*, *N*, *S*, *E*, *W* - point of interest, north standing for the positive *y*-direction, south for the negative *y*-direction, east for the positive *x*-direction, and west for the negative *x*-direction. The lower case letters *n*, *s*, *e*, *w* denote the control volume faces at north, south, east, and west, respectively.

The governing differential equation for the diffusion in porous solid, Eq. (20), is parabolic in time (t) and elliptic in space (y). Time is discretized using Euler backward differencing, which is implicit and first order accurate. For space discretization, the second-order central difference scheme was applied. The governing equations for convective mass transfer presented in Eq. (19) are parabolic in time and along the flow direction (i.e., x-direction), and elliptic in the y-direction. As for time integration, the Euler backward differencing scheme was used to advance the solution in time while integration in the x-direction is performed using the Crank-Nicolson method, which is implicit and second order accurate, so that all spatial derivatives are second order accurate. As for the y-direction, the central difference scheme was used.

Applying those schemes, the discretization equations can be generalized as

$$a_P\cdot\theta_P = a_N\cdot\theta_N + a_S\cdot\theta_S + a_W\cdot\theta_W + a_{WN}\cdot\theta_{WN} + a_{WS}\cdot\theta_{WS} + a_P{}^0\cdot\theta_P{}^0 \quad (29)$$

where, superscript ^{0} denotes for previous time step. The coefficients for convection and diffusion of both models are summarized in Table 1. Models 1 and 2 refer to the conjugate mass transfer models with quasi-steady convection and unsteady convection, respectively.

The boundary conditions of no mass flux at the edges of solid (at $x = 0$, $x = L$) and the bottom of solid (at $y = -b$), can be easily implemented using the half control volume [Patankar, 1980]. At the solid-fluid interface, the concentration and the mass flux are continuous as given in Eqs. (23) and (24). The continuity of the concentration was implemented by locating the control volume face at the interface. The mass flux continuity was enforced by calculating the interface diffusivity as the harmonic mean of solid diffusivity and fluid diffusivity [Patankar, 1980].

In this study, a finer grid was used where the concentration gradient is large, i.e., near the leading edge ($x = 0$) and near the interface in both fluid and solid fields ($y = 0^+$ and $y = 0^-$). Since the physical space is rectangular, three orthogonal one-dimensional algebraic transformations (i.e., *x*-direction in whole field, *y*-direction in fluid field, and *y*-direction in solid field) were applied using a hyperbolic stretching function. The time step Δt was set such that the time and space errors are of the same size. Note that, since the Euler implicit scheme is used in time discretization, there is no stability limitation on the size of time step Δt. For every case considered, several tests with different time steps were carried out.

In the discretization equation for Models 1 and 2, θ_P depends on θ_N, θ_S, θ_W, θ_{WN} and θ_{WS}, but not on θ_E. In other words, *x*-coordinate becomes a one-way coordinate and only *y*-coordinate is a two-way coordinate, which can be solved by a marching

procedure along *x*-direction [Patanka, 1980]. The Thomas algorithm can directly solve a tridiagonal matrix formed in *y*-coordinates at each station along the *x*-direction, i.e., line-by-line method.

The developed codes were tested at various levels. At first, the codes for diffusion in solid and for convection in fluid were tested separately by comparing the results with analytical ones [Ozisik, 1980, White, 1991]. Then, the steady state solutions of unsteady conjugate mass transfer, where unsteady two-dimensional convection coupled with unsteady one-dimensional diffusion in solid, were validated with the steady conjugate heat transfer numerical solution by Yu et al. (1991) through a heat-mass transfer analogy.

RESULTS AND DISCUSSION

The numerical computations were carried out for various ranges of the independent variables: Re_L, D_a/D_s, and b/L. Since momentum and mass transfer are affected by convection in the fluid region, two values of Reynolds number, $Re_L = 10^2$ and 10^4, were considered and one value for the Schmidt number (Sc=2.57) was used since Sc varies very slightly from one VOC to another, i.e., 0.9 – 3.1 [Sparks, et al., 1996]. Among the solid material properties, (ε+K) was set as constant since the previous parametric study results showed that the effect of (ε+K) is linear [Lee et al., 2003b]. D_a/D_s was varied in the range of 10 to 10^3; this range was decided based on the previous study, which showed the range of measured D_a/D_s for gas-phase diffusion of various porous building materials are from 4.42 to 255 [Haghighat et al., 2002]. The thickness to length ratio (b/L) was varied from 10^{-3} to 10^{-1}.

Figure 3 presents the effect of Fourier number on $\theta_w(x)$ and Sh_x^+ distributions over x for Bi = 9.1. As Fo increases or time progresses, $\theta_w(x)$ decreases since more and more mass is carried away (for source behavior). This results in the increase of Sh_x^+ with Fo. When Fo is larger than 50, Sh_x^+ decreases near the leading edge and then gradually increases along the down stream. When Fo=100, almost 90% of the initial total mass is already transferred, and the remaining mass to be transferred is least near the leading edge due to higher mass transfer rate there. This may cause more reduction in the concentration gradient in the y-direction relative to the increase of $\theta_w(x)$ in the downstream direction; hence, Sh_x^+ increases in the downstream direction at large Fo.

In unsteady conjugate mass transfer problem (Model 2), two different characteristic time scales are in effect: the convection characteristic time, t_c defined as L/u_∞, and the diffusion characteristic time, t_d defined as b/D_s^2. The ratio of these two values can be an important dimensionless parameter to describe the unsteadiness in conjugate mass transfer. In this study, the ratio of diffusion to convection characteristic time, τ, was adopted.

$$\tau = \frac{t_d}{t_c} = \frac{b^2/D_s}{L/u_\infty} = \mathrm{Re}_L\, Sc \cdot \left(\frac{D_a}{D_s}\right) \cdot \left(\frac{b}{L}\right)^2 \quad (30)$$

$\theta_w(x)$ and Sh_x^+ distributions along the plate length for various Fo are presented in Fig. 4 for Bi = 9.1 and τ = 2.57. Those profiles are different from the profiles of the quasi-steady convection model (Model 1), which are shown in Fig. 3. $\theta_w(x)$ of Model 2 are smaller than that of Model 1 for Fo = 1 or less. Sh_x^+ profiles clearly shows the building up of boundary layer with time especially in the early transfer phase. When the boundary layer is not well developed, it shows high mass transfer rates due to the absence of boundary layer resistance. For example, when Fo = 0.1, the convection time t_c^+ is 0.257 for this case. Then the air from leading edge travels only up to x/L=0.257 and the rest part is in direct contact without any resistance due to convection mass transfer. This would cause an increase in the mass transfer rate, or the Sherwood number.

Figure 5 compares the dependence of $(\theta_w)_{ave}$ and Sh_L^+ on Fo for three different cases of τ with Bi = 9.1 predicted by the unsteady convection model (Model 2), with that by the quasi-steady convection model (Model 1). At larger τ, the differences in $(\theta_w)_{ave}$ and Sh_L^+ between Models 1 and 2 get to be smaller. Although the same range of Fo is considered in all three cases, the convection time, t_c^+ differs up to by the factor of 100, implying that as far as mass convection is concerned, the case of τ = 25.7 behaves more like a quasi-steady convection while the others are unsteady. The difference decreases as time progresses or Fo increases. For τ = 25.7, $(\theta_w)_{ave}$ and Sh_L^+ profiles are similar to those of Model 1. For τ = 2.57, the error in $(\theta_w)_{ave}$ and Sh_L^+ are 0.18 and 0.54, respectively at Fo = 0.2. When Fo is larger than 1.0, the $(\theta_w)_{ave}$ profile follows that of quasi-steady convection model. The difference become significant for τ = 0.257: at Fo = 0.2, $(\theta_w)_{ave}$ is about one third larger and Sh_L^+ is 4.6 times larger compared with the results of Model 1. For Fo larger than 30, the difference becomes negligible.

Table 2 presents the time (expressed in terms of both Fo and t_c^+, and denoted as $(Fo)_{5\%}$ and $(t_c^+)_{5\%}$) that is required to reach less than 5% of error on $(\theta_w)_{ave}$ between Models 1 and 2, for all considered cases of Bi and τ. The results show that the value of $(t_c^+)_{5\%}$ ranges from 0.98 to 2.31, while $(Fo)_{5\%}$ ranges from 4.4×10^{-6} to 897. In other words, quasi-steady convection assumption can be applied after less than

two and half sweeps by the forced flow over the entire plate, but the proportion of this duration to *Fo* depends on τ and varies widely. $(Fo)_{5\%}$ was compared to the time (expressed as Fourier number) required to transfer 99% of total transferable VOC mass, Fo_{total}, which was obtained from the analytical model by Lee et al. (2003). $(Fo)_{5\%}$ can be relatively long for cases of small τ - the maximum is 17.2% of Fo_{total} for $\tau = 2.57\times10^{-3}$. When the characteristic times for convection and diffusion are in the same order, the ratio, $(Fo)_{5\%}/Fo_{total}$ is in the order of 10^{-3}. When τ is larger than that, the ratio $(Fo)_{5\%}/Fo_{total}$ becomes infinitesimal.

CONCLUSION

Numerical conjugate mass transfer models were developed to predict VOC source and sink behavior of porous building materials, and the validity of commonly adopted assumption of quasi-steady convection was examined for inclusive cases of material properties and Reynolds number. The quasi-steady assumption in convection mass transfer may result in significant overestimation of wall concentration or underestimation of Sherwood number in the early transfer phase; however, after less than 2.5 times of convection characteristic time, i.e., the time taken by a particle moving with a velocity of u_∞ to travel along the plate from x=0 to x=L, the quasi-steady assumption is a valid assumption. This duration is equivalent to at most 17.2% of total mass transfer time for cases with convection characteristic time longer than that of diffusion.

ACKNOWLEDGMENT

The authors would like to acknowledge the financial support of the Natural Sciences and Engineering Research Council of Canada (NSERC), EJLB Foundation, and the Institut de Recherche Robert-Sauvé en Santé et en Sécurité du Travail (IRSST)

NOMENCLATURE

English symbols

a	coefficient of discretization equation [-]
b	thickness of solid [m]
C	gas-phase VOC concentration [mg /m^3]
C_{ad}	adsorbed-phase concentration [mg/m^3]
D_a	molecular diffusion coefficient for binary mixture of air and VOC [m^2/s]
D_s	overall effective diffusion coefficient of the solid [m^2/s]
h_D	convection mass transfer coefficient [m/s]
K	Henry adsorption equilibrium constant [-]
L	length of solid [m]
t	time [s].
t_c	convection characteristic time ($t_c = L/u_\infty$) [s]
t_d	diffusion characteristic time ($t_d = b^2/D_s$) [s]
t_{total}	total transfer time [s]
u	velocity component in x-direction [m/s]
v	velocity component y-direction [m/s]
x	coordinate parallel to the wall [m]
y	coordinate normal to the wall [m]

Greek symbols

γ	dimensionless diffusivity, i.e., D_s/D_a for solid and D_a/D_a for air [-]
ε	porosity [-]
ν	kinematic viscosity [m^2/s]
ϕ	thickness (b) to length (L) ratio of solid [-]
θ	nondimensionalized concentration [-]
τ	ratio of diffusion to convection characteristic time [-]

Dimensionless groups

Bi	mass transfer Biot number ($Bi = h_D \cdot b/D_s$)
Fo	Fourier number ($Fo = t \cdot D_s /b^2$)
Re_L	Reynolds number based on the plate length ($Re_L = u_\infty \cdot L/\nu$)
Sc	Schmidt number ($Sc = \nu/D_a$)
Sh_L	averaged Sherwood number ($Sh_L = (h_D)_{ave} \cdot L/D_a$)
Sh_x	local Sherwood number ($Sh_x = h_D \cdot x/D_a$)

Subscripts

∞	far field, i.e., outside the boundary layer
ave	average value
o	initial value at t = 0
w	at the fluid –solid interface
$y=0^-$	at the solid side of the solid-fluid interface
$y=0^+$	at the fluid side of the solid-fluid interface

Superscripts

0	at the time level t
+	dimensionless variable

REFERENCES

Haghighat, F., Lee, C.S., and Ghaly, W.S., "Measurement of diffusion coefficients of VOCs for building materials: review and development of a calculation procedure", *Indoor Air*, vol.12, pp. 81-91, 2002

Huang, H., and Haghighat, F., "Modeling of volatile organic compounds emission from dry building materials", *Building and Environment*, vol. 37, no. 11, pp. 1127-1138, 2002

Lee, C.S., Haghighat, F., and Ghaly, W.S., "Source and Sink Behaviours of Porous Building Materials: Part I – Model Development and Validation", *Proceedings of Healthy Building 2003*, vol. 1, pp. 355-360, Singapore, December 7 – 11, 2003a

Lee, C.S., Haghighat, F., and Ghaly, W.S., "Source and Sink Behaviours of Porous Building Materials: Part II – Effects of Reynolds Number and Temperature", *Proceedings of Healthy Building 2003*, vol. 1, pp. 361-366, Singapore, December 7 – 11, 2003b

Meininghaus, R., Gunnarsen, L., and Knudsen, H.N., "Diffusion and sorption of volatile organic compounds in building materials-impact on indoor air quality", *Environmental Science & Technology*, vol.34, pp.3101-3108, 2000

Özisik, M.N., *Heat Conduction*, John Wiley & sons, Inc., 1980

Patankar, S.V., *Numerical Heat Transfer and Fluid Flow*, Hemisphere Publishing Corp., Washington D.C., 1980

Sparks, L. E., Tichenor, B. A. and Guo, Z, "Gas-phase mass transfer model for predicting volatile organic compound (VOC) emission rates from indoor pollutant sources", *Indoor Air*, vol. 6, pp. 31-40, 1996

White, F.M., *Viscous Fluid Flow*, 2nd edition, McGraw-Hill, New York, 1991

Yu, W.-S., Lin, H.-T. and Hwang, T.-Y., "Conjugate heat transfer of conduction and forced convection along wedges and a rotating cone", *Int. J. of Heat Mass Transfer*, vol. 34, no. 10, pp.2497-2507, 1991

Table 1. Coefficients of discretization equations for Model 1 and 2

Discretization equation

$$a_P \cdot \theta_P = a_N \cdot \theta_N + a_S \cdot \theta_S + a_W \cdot \theta_W + a_{WN} \cdot \theta_{WN} + a_{WS} \cdot \theta_{WS} + a_P^{\,0} \cdot \theta_P^{\,0}$$

with $a_P = a_P^{\,0} + a_N + a_S + a_W + a_{WN} + a_{WS}$

Model no.	**Coefficient**	**Diffusion in solid ($\gamma = D_s/D_a$)**	**Convection in fluid ($\gamma = D_a/D_a = 1$)**
1	a_N	$\Gamma_n = \dfrac{\gamma}{\phi^2 \,\mathrm{Re}_L \, Sc \cdot \delta y_n}$	$0.5\delta x_w \cdot (-F_P + \Gamma_n)$; where, $F_P = \dfrac{v_P}{2\phi}$
	a_S	$\Gamma_s = \dfrac{\gamma}{\phi^2 \,\mathrm{Re}_L \, Sc \cdot \delta y_s}$	$0.5\delta x_w \cdot (F_P + \Gamma_s)$
	a_W	0	$0.5 \cdot [(u_P + u_W) \cdot \Delta y - (\Gamma_n + \Gamma_s) \cdot \delta x_w]$
	a_{WN}	0	$0.5\delta x_w \cdot (-F_W + \Gamma_n)$; where, $F_W = \dfrac{v_W}{2\phi}$
	a_{WS}	0	$0.5\delta x_w \cdot (F_W + \Gamma_s)$
	$a_P^{\,0}$	$(\varepsilon + K)\dfrac{\Delta y}{\Delta t}$	0
2	a_N	Γ_n	$0.5\delta x_w \cdot (-F_P + \Gamma_n)$
	a_S	Γ_s	$0.5\delta x_w \cdot (F_P + \Gamma_s)$
	a_W	0	$0.5 \cdot [(u_P + u_W) \cdot \Delta y - (\Gamma_n + \Gamma_s) \cdot \delta x_w]$
	a_{WN}	0	$0.5\delta x_w \cdot (-F_W + \Gamma_n)$
	a_{WS}	0	$0.5\delta x_w \cdot (F_W + \Gamma_s)$
	$a_P^{\,0}$	$(\varepsilon + K)\dfrac{\Delta y}{\Delta t}$	$\dfrac{\Delta y \cdot \delta x_w}{\Delta t}$

Table 2. Time to reach less than 5% of error between $(\theta_w)_{ave}$ by Models 1 and 2

Denote	Bi	τ	**time required to reach error < 5%**		
			$(t_c^+)_{5\%}$	$(Fo)_{5\%}$	$(Fo)_{5\%}/Fo_{total}$
Bi = 0.091	9.0952×10^{-2}	2.57×10^{-3}	2.31	8.97×10^{2}	1.72×10^{-1}
Bi = 0.91a	9.0952×10^{-1}	2.57×10^{-2}	1.71	6.65×10	1.00×10^{-1}
Bi = 0.91b	9.0952×10^{-1}	2.57×10^{-1}	1.76	6.83	1.03×10^{-2}
Bi = 9.1a	9.0952	2.57×10^{-1}	0.98	3.79	1.70×10^{-2}
Bi = 9.1b	9.0952	2.57	1.63	6.32×10^{-1}	2.83×10^{-3}
Bi = 9.1c	9.0952	2.57×10	1.75	6.81×10^{-2}	3.05×10^{-4}
Bi = 91a	9.0952×10	2.57×10	1.00	3.87×10^{-2}	2.12×10^{-4}
Bi = 91b	9.0952×10	2.57×10^{2}	1.62	6.28×10^{-3}	3.44×10^{-5}
Bi = 91c	9.0952×10	2.57×10^{3}	1.75	6.79×10^{-4}	3.72×10^{-6}
Bi = 910a	9.0952×10^{2}	2.57×10^{3}	1.14	4.42×10^{-4}	2.47×10^{-6}
Bi = 910b	9.0952×10^{2}	2.57×10^{4}	1.58	6.15×10^{-5}	3.44×10^{-7}
Bi =9100	9.0952×10^{3}	2.57×10^{5}	1.13	4.40×10^{-6}	2.47×10^{-8}

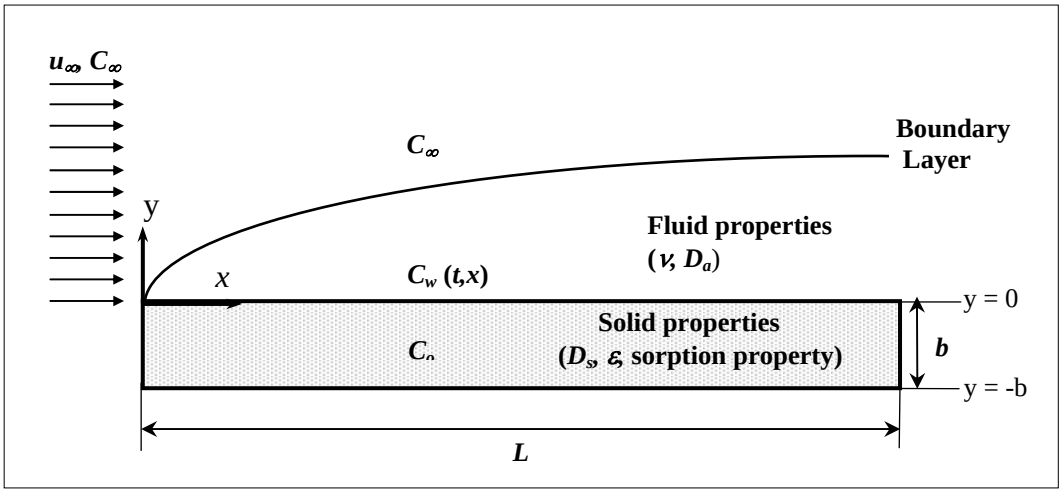

Figure 1 Schematic diagram of the conjugate mass transfer problem

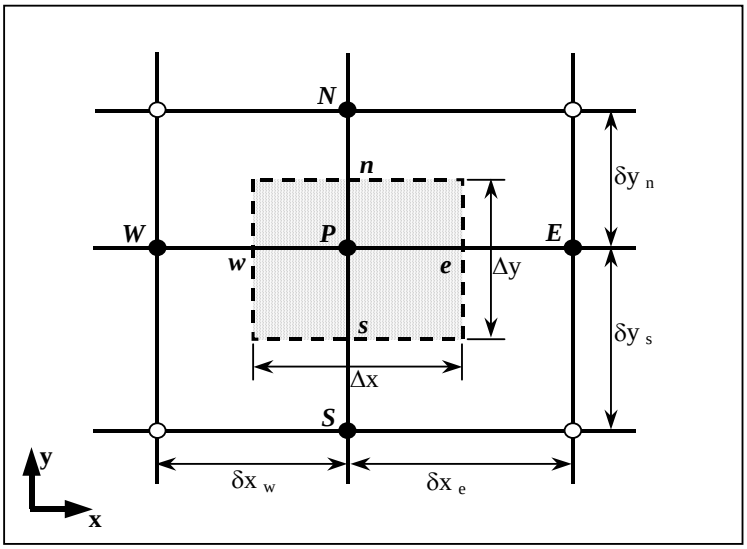

Figure 2 Control volume

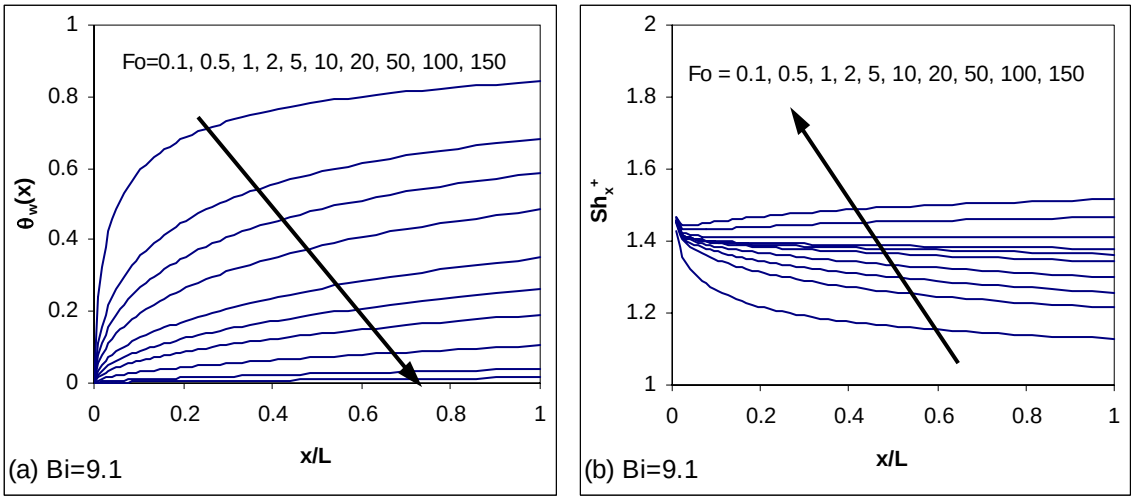

Figure 3 Wall concentration and local Sherwood number profile for Bi=9.1 by Model 1

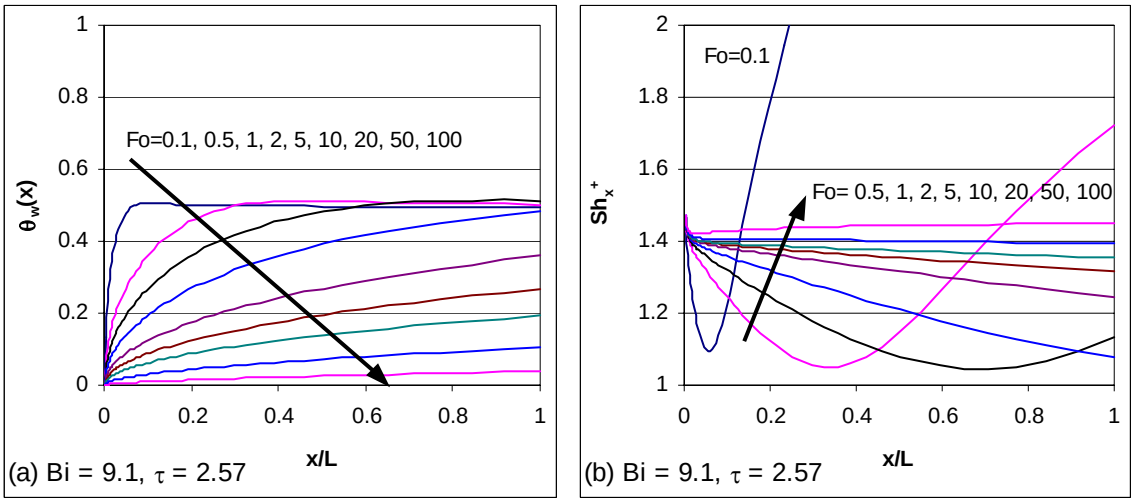

Figure 4 Wall concentration and local Sherwood no. profile for Bi=9.1 and τ =2.57 by Model 2

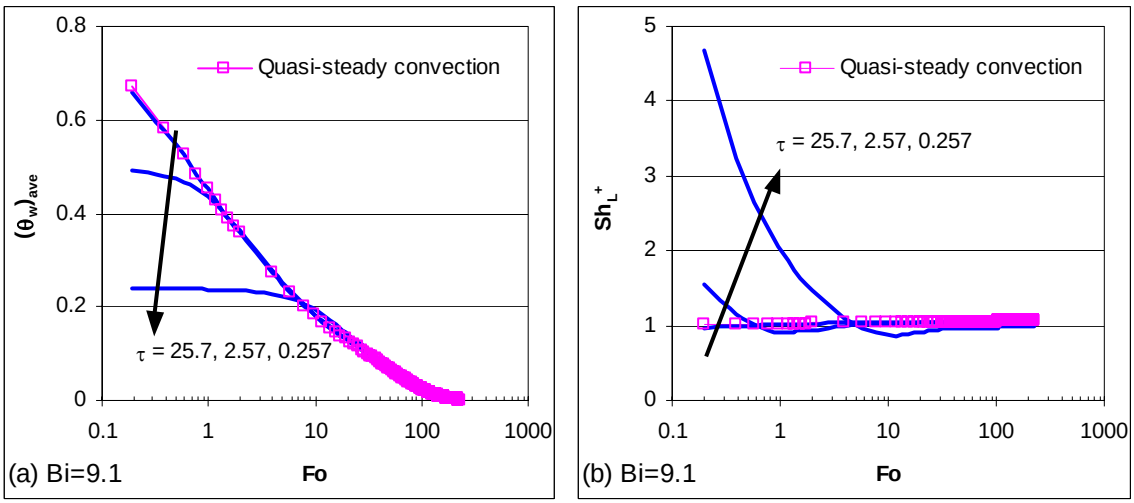

Figure 5 Dependence of averaged wall concentration and averaged Sherwood no. on Fourier no. for different τ